Tanzania Journal of Science

Volume 51(3), 2025





Design of high-performance synchronous reluctance motor for hybrid electric vehicle application

Fredy F Loita^{1,2*} and Jackson J Justo^{1,3}

Keywords

Reluctance motor; rotor reluctance torques; electric vehicle; finite element analysis

Abstract

This paper presents the simulation-based design of a synchronous reluctance motor (SynRM) coupled electromechanical system suitable for the hybrid electric vehicle. The study considers SynRM with a 75kW power rating with the capability to produce up to 125kW maximum power for the electric vehicle. The focus is mainly on rotor and stator design; the angles of the flux-barrier ends are considered to reduce the torque ripple due to the slot harmonics. Reluctance machines are indeed competitive for applications requiring high efficiency at low cost. However, it is a challenging task to find design solutions that ensure structural integrity of the motor without compromising its overall performance, particularly in the presence of optimized rotor flux barriers. The impact of electrical design on the mechanical characteristics of the rotor is discussed as well. The overall design and comprehensive of electromagnetic finite element analysis are conducted using Ansys Motor CAD software. In the results analysis, the predicted mechanical characteristics of the reluctance motor, such as torque versus speed behavior, power losses, and power factor, are presented. The efficiency map of the designed SynRM is also discussed in the whole operating region, indicating a high performance is achieved as compared to the existing design. The absence of rotor winding in the robust rotor design and proper arrangement flux barrier has led to more than 30% reduction in copper losses, improved thermal performance, increased mechanical robustness, and simplified manufacturing processes compared to the induction motor. Compared to similarly size Synchronous motor, the proposed design exhibits consistently superior efficiency beyond 1,000 rpm, delivering relatively 18% and 43% higher power output at 4,000 rpm and 8,000 rpm, respectively

Introduction

The origin of synchronous reluctance machines dates back to their invention by Kostko in 1923. However, they remained largely unused as motors until the late 1970s,

primarily due to the complexity of the power electronics required for their control (Ayad et al. 2018). In recent years, these machines have gained growing attention in both industrial and automotive sectors. Compared

Received 6 April 2025, Revised 21 Aug 2025, Accepted 19 October 2025, Published 30 October 2025 https://doi.org/10.65085/2507-7961.1055

© College of Natural and Applied Sciences, University of Dar es Salaam, 2025 ISSN 0856-1761, e-ISSN 2507-7961

¹Department of Electrical Engineering, University of Dar es Salaam, P. O. Box 35091, Dar es Salaam, Tanzania; justo.jack@udsm.ac.tz, ORCID: https://orcid.org/0000-0003-0638-0713

 $^{^2} Department\ of\ Electrical\ and\ Power\ Engineering,\ Mbeya\ University\ of\ Science\ and\ Technology,$

P. O. Box 131, Mbeya, Tanzania; fredyloita@gmail.com, ORCID: https://orcid.org/0009-0009-3831-3639 ³Faculty of Control Systems and Robotics, ITMO University, St. Petersburg, Russia

^{*}Corresponding Author Email: fredyloita@gmail.com

to induction motors and permanent magnet synchronous machines (PMSMs) equivalent power ratings, synchronous reluctance machines offer comparable performance without relying on costly copper bars or rare-earth magnets (Kim, high efficiency ((2019)).Their mechanical robustness across a wide speed range make them a compelling alternative for applications, various including vehicles and traction systems (Myint, 2018).

The potential scarcity or high cost of rare earth magnets has raised concerns about the availability and affordability of interior permanent magnet synchronous synchronous (IPMSMs). As a result, reluctance motors are becoming increasingly attractive for use in electric and hybrid electric vehicles (EVs and HEVs) due to their robust, simple construction and safe, magnetfree operation (Kuci et al. 2020). In light of these advantages, a reluctance (REL) motor has been developed for an electric-assisted bicycle. The design focuses primarily on reducing torque ripple and enhancing efficiency across a broad speed range.

To achieve this goal, an analytical approach has been implemented to improve the rotor geometry (Ozcelik, et al. 2019). Most studies either focus on analytical models or specific aspects of design. The researchers and experts provide insights into the design of SynRMs with single-tooth windings(Hu et al. (2021); Hua, et al., (2021) C. T. Liu et al., (2019), Z. Liu, et all. (2021)).

While significant research has focused on SynRM design, there is a continued need for optimized designs specifically tailored for the demanding power and torque requirements, as well as wide operating speed ranges, of modern hybrid electric vehicles, particularly concerning the reduction of torque ripple while maintaining structural integrity at high speeds. This paper bridges the gap by presenting a comprehensive simulation-driven design and analysis workflow for a highpower SynRM, addressing key performance indicators relevant to HEV applications. The design focus more on the geometric design of the rotor and stator. The parameter design, optimization and performance validation are

carried out using advanced commercial simulation software (Ansys Motor CAD). The software moves beyond simple analytical formulas by performing complex FEA, allowing for the accurate consideration of non-linear magnetic behavior, saturation, and intricate geometries. The analysis of the torque characteristics of a SynRM model demonstrates its ability to predict motor performance under various operating conditions. Moreover, the study analyzes the performance characteristics of the designed motor to suit the specified application. On the rotor geometry, the angles of the flux-barrier ends are considered to reduce the torque ripple due to the slot harmonics. The paper proposed a novel rotor structure for mediumspeed SynRMs to be tested alongside a common rotor structure.

This study Systematic design of SynRM is explained in section III, geometry design of rotor and stator configurations is presented in Section IV, while a specific rotor and stator arrangement is detailed. Section V addresses the analysis of Motor performance and analysis. Section VI provides an accurate analysis of the final configuration of the REL motor.

Torque Production of SynRM

synchronous reluctance machine utilizes the concept of reluctance and rotating sinusoidal magneto motive force (MMF), which can be generated by the traditional IM stator, for torque production. The main idea can be illustrated by Figure 1. A magnetic field (Ψ) applied to the anisotropic object produces torque when there is an angle difference between the d-axis and the field. It is evident that if the d-axis of the object is not aligned with the field, it will introduce a field distortion in the main field (Wang, et al. 2017). The primary direction of this distorted field is aligned along the object's q-axis. The synchronous reluctance motor employs a sinusoidally distributed winding housed in a slotted stator, with a small air gap linking the stator and rotor similar to a conventional induction motor (Dursun et al. 2023). As the name suggests, the magnetic field rotates at synchronous speed and is typically assumed to have a sinusoidal distribution. Under these

conditions, a constant torque acts to minimize the system's potential energy by reducing field distortion along the q-axis. When the load angle is held steady either through control strategies or by applying a load torque electromagnetic energy is continuously converted into mechanical energy (Tursini et al. 2018). In this setup, the stator current serves a dual purpose: providing magnetization and generating torque, both of which aim to minimize field distortion. This is achieved by controlling the current angle,

which defines the angle between the stator current vector and the rotor d-axis in the synchronous reference frame. In this frame, the synchronous reluctance motor features two distinct rotor flux paths: the d-axis path, which offers high magnetic permeability as flux travels through the rotor iron parallel to the flux barriers, and the q-axis path, characterized by low permeability, requiring the flux to cross the rotor's flux barriers. These orthogonal flux paths form the basis of the final dq synchronous reference frame.

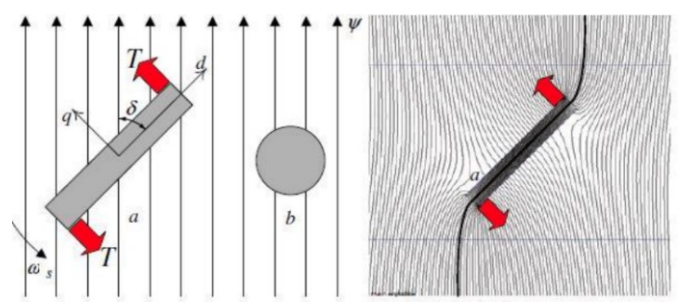


Figure 1: Anisotropic geometry to show the difference in the flux encounters with the magnetic object to produce reluctance torque

The rotor is designed with several flux barriers to obstruct the flux along the q-axis and achieve a high saliency ratio, which corresponds to a high reluctance torque component (Hu, et al. 2020). The iron bridges, located at the ends and sometimes in the middle of each barrier, support the rotor parts. A portion of the q-axis flux flows through these bridges, resulting in a reduction of the torque. Figure 2 shows diagrams of the SynRM geometry, along with their d- and q-axes flux lines.

The electromagnetic torque T_{em} depends on the saliency ratio and has higher values for higher values of the saliency ratio ξ . The electromagnetic torque can be expressed as

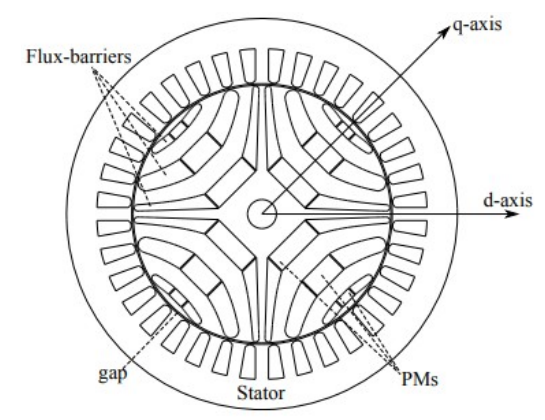
$$T_{em} = \frac{3}{2} n_p L_d \left(1 - \frac{1}{\xi} \right) I_d I_q(1)$$

where, I_d and I_q , d-axis and q-axis current components, respectively.

seen from equation (1),electromagnetic torque is directly influenced by the saliency ratio. Over the past decade, significant research efforts have focused on enhancing this ratio. The saliency ratio is determined by the anisotropic design of the rotor various rotor geometries vield different saliency ratios, which in turn affect the torque production capability of the machine. It is also conferred in the literature that the saliency ratio can be elevated by inserting low-cost ferrite magnets in the flux barrier path (Kocan, et al. 2021). The saliency ratio can be expressed as

$$\xi = \frac{L_d}{L_a}(2)$$

where L_d and L_q are the d-axis and q-axis inductances, respectively.



(a) flux barrier and axis arrangement.

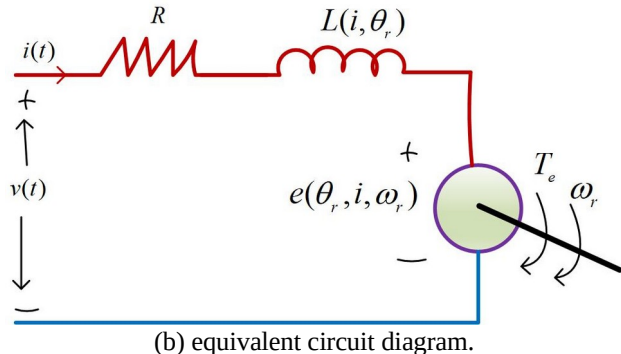


Figure 2: SynRM geometry with its d- and q-axes flux lines (Yamazaki, Kato, Ikemi, & Ohki, 2014)

Systematic Design of SynRM

The design process of the high-performance Synchronous Reluctance Motor for HEVs applications commenced with the establishment of detailed performance specifications, as outlined in

. The complete design flow chat is shown in *Figure 3*, Initial analytical calculations, utilizing established electromagnetic equations, provided foundational parameters for the stator and rotor geometries. However, to account for the complex non-linear magnetic behavior, saturation effects, and intricate flux barrier designs crucial for torque ripple reduction, the design was rigorously developed and analyzed using Ansys Motor-CAD software. This comprehensive computational tool employs FEA to accurately simulate the motor's electromagnetic performance. Within Motor-CAD, the proposed SynRM geometry, including the multi-layered flux barriers and their optimized angles (as depicted in

and Figure 8), was meticulously modeled. The software facilitated the evaluation of critical performance metrics, such as flux distribution (Figure 13), torque production (Figure 15), and efficiency maps, by applying appropriate boundary conditions and considering the material properties shown in Figure 9. The optimization of specific

geometric features, particularly the angles of the flux-barrier ends, was an iterative process performed within Motor-CAD's environment, aimed at achieving a high saliency ratio while effectively minimizing torque ripple due to slot harmonics, thereby enhancing the overall performance suitability for HEV applications.

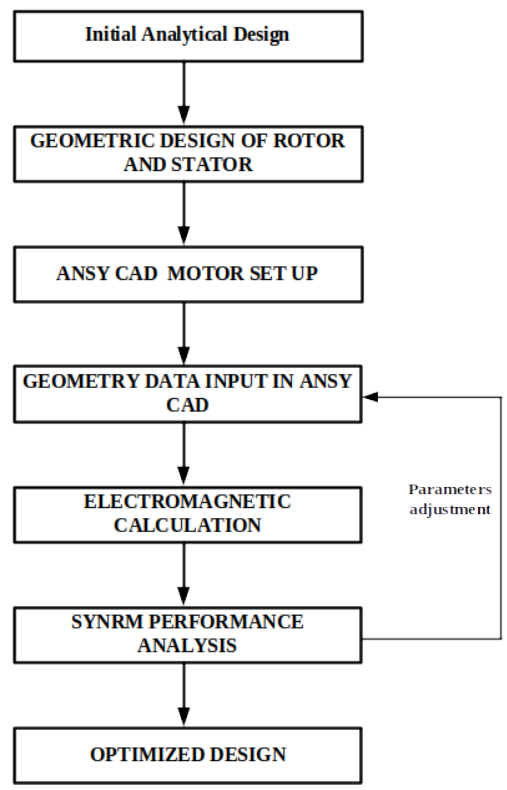


Figure 3: Simulation based Design Flow Chat of SynRM

Table 1: SynRM required specifications

Property	Unit	Value
Max. Output	Kw (hp)	125 (175)
Rated output/at	Kw(hp)/	75 (102)/8000
	rpm	
Torque/at	Nm/AT	125/0
Recuperation output	kW	Up to 50
Number of phases	m	3
Motor technology	Classical synchronous reluctance motor	

Geometry Design of SynRM

The stator structure of the transversally laminated type is essentially the same as that of other machines, such as induction machines, so the main performance difference comes from the rotor structure. The SynRM can be built by putting a reluctance rotor inside stators extracted from an induction production line. The parameters of a Synchronous Reluctance Motor (SynRM) are typically categorized into three main classes: stator design parameters, design variables (or microscopic parameters), and target variables (Aghazadeh et al. 2019). The first category includes geometric features of the stator, such

as the number of slots and poles, as well as the outer and inner diameters. The second category focuses on variables primarily related to rotor geometry. To achieve accurate performance predictions, both the rotor design variables and the target variables must be evaluated using the finite element method (FEM). Structurally, the stator of a SynRM with transverse laminations is similar to that of other machines like induction motors, meaning the key performance distinction lies in the rotor configuration(Credo & Pescetto, (2020); Jung et al., (2015)). In fact, a SynRM can be constructed by inserting a reluctance

rotor into stators originally intended for use in induction motor production lines.

The analytical equations explained in this article serve as initial design guidelines of the SynRM design, but the actual performance analysis and optimization are carried out using the FEA capabilities of Ansys Motor-CAD. The finite element model considers the nonlinear magnetic behavior of the stator and rotor laminations and that the torque is computed using the Maxwell stress tensor in the air gap, where numerical errors related to remising are minimized through a moving band method, keeping the rotor and stator meshes unchanged.

Design Consideration of Stator Geometry

The voltage ratings of the stator is important in the initial design of the motor (Dursun et al., 2023). The value of the voltage affects the insulation of the stator windings. The higher the value, the higher the insulation required. The higher insulation increases the size and manufacturing cost of the motor. so the optimal design is needed. The rated voltage depends on the amount of flux per pole, winding factor (K_w) , Frequency (f), and number of turns of main winding (N_m) , see (3).

$$V = 4.44 K_w f \varnothing N_m(3)$$

The flux per pole is important in the saliency ratio of the motor. It initially considered for the initial design of the SynRM. The flux per pole can be obtained by considering the average value of flux density in the air gap (B_{av}), the number of poles (P), the stator core length (L), and the stator bore diameter (D). See equation (4). Also, the ampere conductor per meter of arm periphery is given by equation (5). Ampere conductor per meter essential in determining the MMF produced by the winding, which in turn dictates the magnetic field strength and ultimately the motor's performance.

$$\varnothing = B_{av} \frac{\pi D}{P} L(4)$$

$$ac = \frac{2 N_m I}{\pi D} (5)$$

$$KVA = C_o \times D^2 L n_s(6)$$

$$C_o = 1.11 \pi^2 K_w B_{av} \times ac \times 10^{-3}$$

where C_o is the output coefficient.

In the initial design of an electric machine, two key factors are pole pitch (T_P) and width of the teeth (b_{t1}). The magnetic poles spacing around the machine i.e. pole pitch, which is crucial for establishing the magnetic field, influencing how the machine produces torque, and affecting the winding design (Tursini et al., 2018). The width of the teeth, which are the core sections between the winding slots, is vital for ensuring sufficient space for magnetic flux without saturation, providing adequate room for windings to minimize losses, and maintaining the mechanical strength of the core. Both parameters are interconnected and must be carefully balanced achieve the desired performance, efficiency, and structural integrity of the machine. The pole pitch, width of the teeth, and depth of the stator core (dc1) are obtained by equations (7) - (9) below.

$$T_{p} \cong L = \frac{\pi D}{P}(7)$$

$$d_{c1} = \frac{b_{t}}{b_{s}} \times \frac{S_{1} \times b_{t1}}{\pi P}(8)$$

$$b_{t1} = \frac{\left(1.27 \times 0.035 D_{i}\right) D_{i}}{S_{s}}(9)$$

The length of the air gap, the small space between the rotor and stator, is a critical initial design choice for the motor. A shorter air gap generally leads to a stronger magnetic field and higher torque output for a given current, but it also increases attractive magnetic forces, which can lead to more noise and vibration. Conversely, a longer air gap reduces the magnetic forces and makes manufacturing tolerances less critical, but it requires a larger magnetizing current to establish the necessary magnetic flux, which can lower the machine's power factor and efficiency (Hua et al., 2021). The carefully balance of electromagnetic and mechanical was considered to optimize the air gap length for reluctance motor performance. The initial analytical length of the air gap, l_q depends on the inner diameter and number pole and is given by (10).

$$l_g = 0.013 + \frac{0.0042 D_i}{\sqrt{P}} (10)$$

The slot dimensions have to be obtained for the stator geometry design. Figure 4 shows the shape of the stator slot. The total number of stator slots N_{st} , the useful area of the slot, and the width of teeth can be obtained from (11) and (12).

$$N_{st}=2n_pqm(11)$$

$$b_{ts} = \frac{b_m \times \tau_s}{b_{ts} K_{Fe}} (12)$$

where $b_m \wedge \tau_s$ are tooth flux density and slot pitch, respectively. To reduce the flux ripple, the least possible dimension for slot opening was selected, for this case $2\,mm$, $h_{so} = 1\,mm$ and $h_{s1} = 2\,mm$, while the dimension of b_{s1} , b_{s2} , $h_{s2} \wedge h_{cs}$ can be obtained from (13) – (16) respectively.

$$b_{s1} = \frac{\pi}{N_s} \left(D_{ro} + 2 h_{s0} + 2 h_{s1} \right) - b_{ts} (13)$$

$$b_{s2} = \sqrt{\left(4 A_{su} \tan \frac{\pi}{N_s} \right) + b_{s1}^{2}} (14)$$

$$h_{s2} = \frac{2 A_{su}}{b_{s1} + b_{s2}} (15)$$

$$h_{cs} = \frac{B_m \tau}{B_{s2}} (16)$$

Hence, the inner (D_{in}) and outer (D_{out}) diameter of the stator core can be obtained from (17) - (18).

$$D_{i} = D_{ro} + 2g(17)$$

$$D_{out} = D_{i} + 2(h_{so} + h_{s1} + h_{s2} + h_{cs})(18)$$

The after balancing torque and efficiency through optimized parameters such as pole pitch, teeth width, and slots dimensions the motor optimized parameters corresponding to the SynRM requirements were selected as the optimal solution, the parameters listed in Table 2

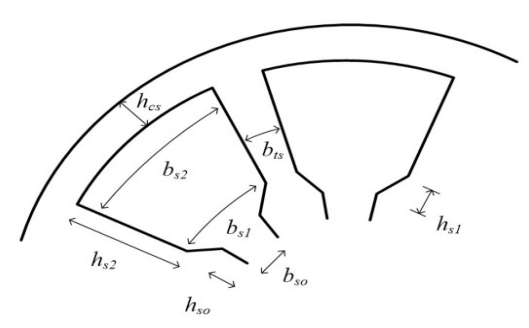


Figure 4: Geometry of the stator dimensional slots considered while optimizing the size air gap and pole pitch.

Table 2:Optimized Stator parameter		
Stator Parameters	Value	
Slot Number	48	
Stator Lam Diameter	200 mm	
Stator Bore	115 mm	
Tooth Width	7 mm	

Slot Depth	30 mm
Slot Corner Radius	1 mm
Tooth Tip Depth	1 mm
Slot Opening	2 mm
Tooth Tip Angle	30°
Sleeve Thickness	0.6 mm (banding thickness)

Design Consideration of Rotor Geometry

To address the structural limitations of synchronous machines in variable-speed applications, several strategies have been employed, including the use of solid rotor structures, external rotor sleeves, dual-state soft magnetic materials, and high-strength soft magnetic materials (Abid, Shah, Zanjani, Leghari, & Bhatti, 2020). Among these, only the approach using high-strength soft magnetic materials avoids the need for specialized manufacturing processes, as it utilizes commercially available materials. While each method helps reduce mechanical stress on iron bridges, solid rotor structures

suffer from significant rotor losses that impair performance. Similarly, using an external sleeve increases the physical air gap, and dual-state materials are costly and not readily available (Credo & Pescetto, 2020). Previous mechanical models have simulated οf laminations behavior rotor under centrifugal forces caused by rotation. However, these models typically assume the laminations start in a stress-free state, overlooking the residual stress introduced during assembly. This oversight contributes to the limited accuracy of existing models.

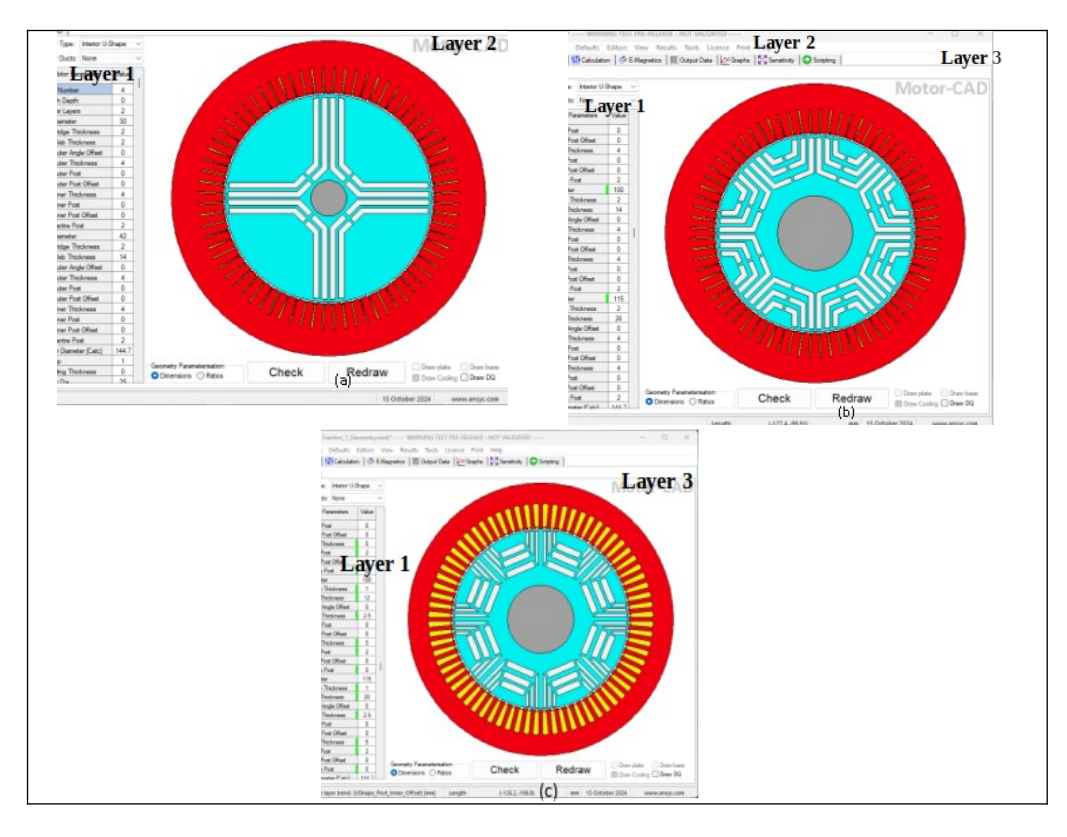


Figure 5: Geometrical diagram of the rotor when different dimensions are optimized to size the flux barriers and improve the motor performance

The rotor of SRM is highly dependent on the so-called ribs. The ribs affect motor speed, torque and even power factor. As the speed increases these ribs are made to be wider for the sake of the rotor robustness but at the cost of a reduction in torque and power factor (Aghazadeh et al., 2019). Several design attempts have been made in order to obtain the required specs of the motor based on analytical rules to design the iron bridge dimensions. From Figure 5 the rotor flux barrier optimized to get high performance reluctance synchronous motor. Figure 4(a), two layer of flux barrier with 18mm slots depth, 7mm tooth width, 0 slots corner radius was analyzed. This design of flux barrier increases torque harmonics and increases the power losses. The flux barrier was then adjusted based of the initial analytical rotor

equations to 3 layers, 20 slots depth and 1 slot corner radius see figure 4(b). However, such analytical models cannot predict the subdivision between the tangential and radial ribs and the positions of the latter along the flux-barrier (Duc, et al. 2023). performance of the motor was increasing by 18% of the first design but fail to achieve the required torque and power performance of the SynRM. It has been shown that the position of the radial ribs plays a key role in the minimization of the maximum stress. The simulation-based design analysis continued until the optimized design (see figure 4(c)) obtained. However, such results are obtained via a parametric study which obviously does not take into account the interaction of all parameters on the structural performances.

Furthermore, the rotor tangential and radial ribs provide mechanical support to the rotor's laminations, particularly at high rotational speeds, see Figure 6. Without these bridges, the segments of the rotor between the flux barriers would not be structurally robust (Kuci et al. 2020). As speed increases, these ribs are often made wider to enhance rotor's robustness and withstand the centrifugal forces. While essential mechanical strength, these iron bridges can negatively affect the motor's electromagnetic

performance. A portion of the q-axis magnetic flux tends to flow through these bridges, which acts as a short-circuit for the flux, thereby reducing the magnetic anisotropy. This reduction in anisotropy can lead to a decrease in both the motor's torque production and its power factor. The optimal design of the SynRM rotor involves position of tangential and radial ribs, multilayer flux carriers and flux barriers.

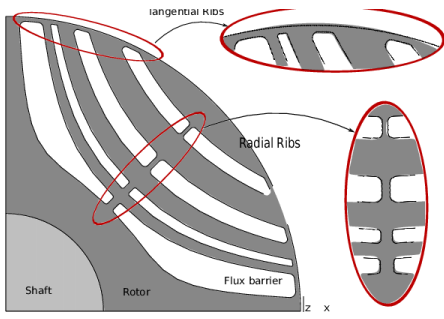


Figure 6: Rotor integrity of modern SynRM to show the position of tangential and radial ribs (Duc et al., 2023)

This anisotropic structure of rotor creates two reluctance paths in the rotor one is high reluctance (along q-axis) and the other one is low reluctance (along d-axis) which results in the production of motor torque. Rotor outer diameter (*D*) is calculated by (19).

$$D_{ro} = 2 n_p \frac{\tau}{\pi} (19)$$

The pole pitch (τ) is the function of electromagnetic torque, d-axis component of air-gap flux density, saliency ratio, pole pairs, stack aspect ratio, cater coefficient, and saturation factor. The length of the rotor (L) can be obtained from the stack aspect ratio, similarly, the length of air-gap (l_g) can be obtained from equation (7) – (10).

Rotor laminations with Joukowski-type flux-barriers (FB) were considered during Table 3 presents the rotor optimized rotor

Table 3: Optimized Rotor parameters

parameter of the SynRM.

intersecting flux barriers, an indirect parameterization is adopted that ensures non-intersecting constraints are always fulfilled. flux-barrier positions and thicknesses are determined by several constructive geometrical points that cannot meet. The idea of the indirect parametrization is to create a network of virtual springs that connect these

designing. In order to prevent the optimizer

from testing sets of parameters corresponding

to erroneous geometries, i.e., geometries with

from each other (Zhu, et al. 2018). An advantage of this method is that all design parameters are of the same nature (whereas geometrical parameters are lengths or angles), which acts as an implicit normalization of the design space.

constructive points in order to repel them

Rotor Parameters	Value
Pole Number	4
Notch Depth	0

Barrier Layers	3
L1 Diameter	60 mm
L1 Bridge Thickness	1.5 mm
L1 Web Thickness	2 mm
L1 Outer Angle Offset	0
L1 Outer Thickness	5 mm
L1 Outer Post	2 mm
L1 Inner Post	2 mm
L1 Inner Post Offset	0
L1 Centre Post	2 mm
L2 Diameter	80 mm
L2 Bridge Thickness	1.5 mm
L2 Web Thickness	12 mm
L2 Outer Angle Offset	0

In the context of the optimization process, the motor's electromagnetic performance can be accurately assessed using a quasi-static approach (Hua et al., 2021). This method involves supplying the stator windings with predefined three-phase currents and performing simulations at multiple evenly spaced rotor positions over a single pole pitch. Each position is analyzed through a sequence of static simulations, effectively capturing the motor's behavior without requiring a fully dynamic model.

The assumption of is customary in synchronous machine models, and particularly helpful in the context of an optimization, because the magnetic model needs to be evaluated a large number of times. The electromagnetic symmetries are exploited to simulate a quarter of the machine by means of appropriate periodic boundary conditions. The finite element model considers the nonlinear magnetic behavior of the stator and rotor laminations, see

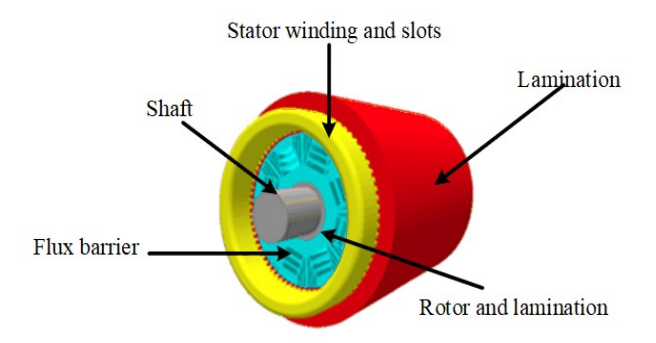


Figure 7: Inner view of the motor geometry simulated in Ansys motor CAD

The hysteretic saturation curve used is that of a M400 50A steel grade, and the nonlinear finite element problem is solved using a Newton-Raphson method. The saturation curve can be modified locally (e.g., in the iron bridges where edge effects are significant) to account for demagnetization effects resulting from manufacturing. The torque is computed using the Maxwell stress tensor in the air gap, where numerical errors

related to remising are minimized through a moving band method, keeping the rotor and stator meshes unchanged. An optimization procedure is required to iteratively update and identify the set of motor parameters by making a trade-off between the different parameters of the machine. In order to reduce the cogging torque, torque ripple, and harmonic components of back electromotive force (EMF), a method of step-skewing rotor

(SSR) is proposed. In this approach, a motor stator are analyzed to compare the with an SSR and another with a slot-skewed performance of each motor.

In this way, the harmonics of back EMF has reduced. The step-skew factors of harmonics are;

$$K_{skew pole v} = \frac{\sin\left(\frac{n.v.a}{2(n-1)}\right)}{nsin\left(\frac{v.a}{2(n-1)}\right)} (20)$$

where n is the number of steps, α is the step skew angle, and v is the order number of harmonic components. The reduction factor of the reluctant torque is

$$K_{skew pole \Re} = \frac{\sin\left(\frac{n \cdot a}{(n-1)}\right)}{nsin\left(\frac{a}{(n-1)}\right)} (21)$$

The torque is finally expressed as

$$T_{em} = \frac{3}{4} n_p I_d I_q L_d \left(1 - \frac{L_q}{L_d} \right) K_{Tskew \ pole \Re} \sin 2\beta \, \mathcal{L}(22)$$

where β is the mechanical angle. Based on equation (22), it can be seen that the step number and step skew angle directly affect the torque and the power density of the motor.

The cross-sectional view of the stator, lamination, and rotor section is shown in Figure 8. The complete 3D view of the designed motor is shown in Figure 9.

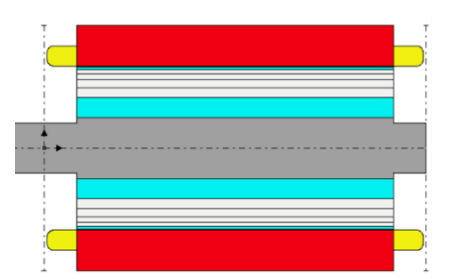


Figure 8: Cross-section view of the motor geometry after obtaining the optimized parameters of the rotor and stator

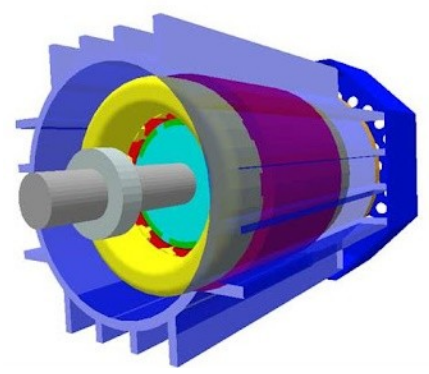


Figure 9: 3D view of rotor and stator geometry in Ansys Motor CAD after obtaining the optimized parameters of stator and rotor

Performance Analysis and Discussion

In the pursuit of designing an optimized synchronous reluctance motor for a hybrid electric vehicle, the Ansys Motor CAD software played a pivotal role in simulating and analyzing the motor's performance. The simulation results of the motor obtained from the software was graphically and analytically analyzed to assess performance of the designed requirements. The subsections below show the graphs of results extracted from Ansys Motor CAD software.

The physical realization of the designed motor that ultimately enables its performance is shown in Figure 9. This figure provides a comprehensive 3D depiction of the complete structure and arrangement of the SynRM. It confirms the physical design being simulated is consistent with the stated parameters and

design principles. It depicts for a clear understanding of the relative positioning of the stator, rotor, windings, and flux barriers, all of which are critical elements influencing how the motor operates magnetically and mechanically.

Electromagnetic performance

Figure 10 illustrates the B-H (Flux Density vs. Magnetic Field Intensity) curves for various steel materials like M250-35A (mild steel), silicon steel, M19 electrical steel, or stainless steel. However, M250-35A electrical steel (dark blue graph) offers superior electromagnetic characteristics compared to mild steel and other materials. This material offers high permeability and high saturation flux density, which are critical for the energy conversion process.

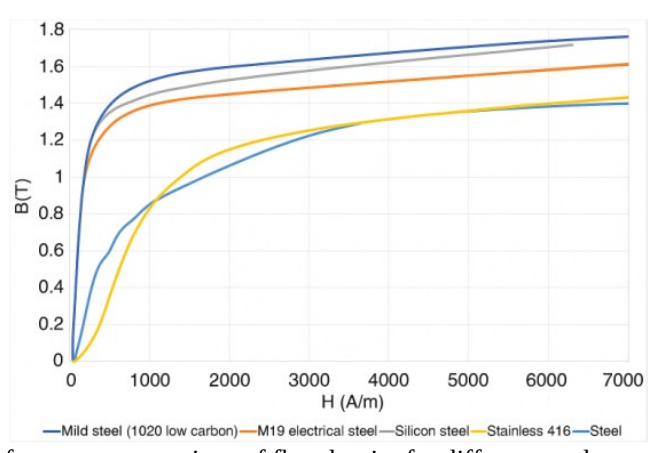


Figure 10: Performance comparison of flux density for different steel materials

high-performance For efficient and synchronous reluctance motors, specialized electrical steels (silicon steels) indispensable. These materials are specifically engineered with high silicon content, low carbon content, and optimized grain structures to achieve low core losses, high permeability, and high saturation flux density, which are critical for the energy conversion process. Therefore. both the rotor and stator laminations made of M250-35A steel for designed motor, with its magnetic flux density and magnetic field intensity values displayed in Figure 10. Beyond approximately H = 2.000 Amps/m, the curve flattens out significantly, indicating that further increases in magnetic field strength (H) result in only minimal increases in flux density (B). This signifies that the material is approaching magnetic saturation. The higher the saturation flux, leading to increased flux density, the M250-35A influences the physical size of the motor and its electromagnetic losses. Moreover, M250-35A is selected because its better torque-to-weight ratio for the motor, which is a vital characteristic for HEVs and even industrial applications.

Effect of harmonic content

Harmonics induce eddy currents in both the stator core and, more significantly, in the rotor laminations (especially the solid parts of the rotor and flux barriers). These losses reduce efficiency and increase operating temperature. The magnitude of these losses is proportional to the square of the harmonic flux density, which is directly influenced by the harmonic winding factor. While less dominant than eddy currents for higher frequencies, harmonic flux components still contribute to hysteresis losses.

The bar graph in *Figure 11* shows the contribution of dominant harmonics in the winding factor, with the analysis indicating less than 5% contribution for higher-order harmonics. This low harmonic content is a significant performance advantage, as higher-order harmonics can lead to undesirable torque ripple, vibrations, acoustic noise, and premature mechanical wear.

$$1^{st} = 0.997 (fundamental)$$

 $5^{th} \wedge 13^{th} = 0.217$
 $7^{th} \wedge 11^{th} = 0.117$

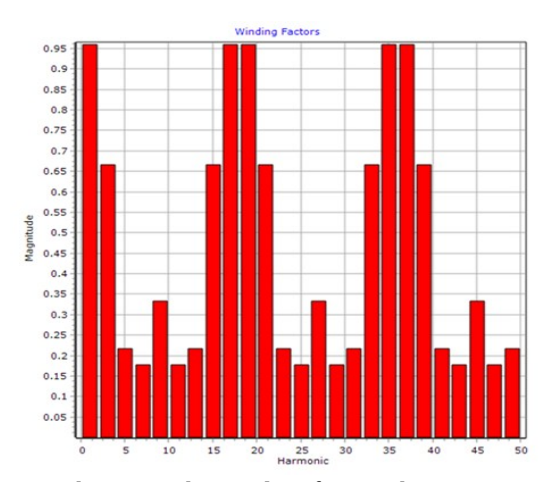


Figure 11: Harmonics contribution in the winding factor when interact with the rotor saliency

Higher-order MMF harmonics interact with the rotor's saliency and other magnetic field harmonics (e.g., due to rotor geometry) to produce undesirable torque ripple. This results in vibrations, acoustic noise, and contributes to premature mechanical wear. Furthermore, minimizing harmonics reduces eddy current and hysteresis losses, thereby improving overall motor performance, efficiency and extending operational lifespan. For a designed SynRM, a winding is designed to minimize the winding factor and allow low-order spatial harmonics.

Variation of flux linkage and flux distribution

Figure 12 is a graph depicting the flux linkage characteristics of a motor over position (angle). Flux linkage refers to the measure of magnetic flux interacting with the coils of the motor. The graph displays flux linkage curves for three phases (six different coils) identified as phase 1, phase 2, phase 3, Phase 1 slice 1, phase 1 slice 2, and phase 1 slice 3. Each phase exhibits a sinusoidal waveform, representing the alternating nature of the magnetic field generated by the motor. The waveforms show a phase shift between the three-phase motor. This phase shift

ensures proper synchronization of the magnetic fields and efficient torque generation. The graph's analysis highlights the sinusoidal variation of flux linkage, initial transients during motor start-up, steady-state operation, and the significance of phase relationships for synchronized magnetic fields.

Figure 13 also shows the distribution of magnetic flux in the rotor geometry. The analysis shows zero distribution (blue color) on the flux barrier and maximum distribution (red color) along the barrier gaps. The difference in flux distribution facilitates torque production.

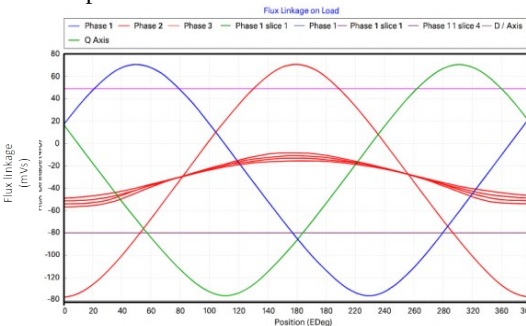


Figure 12: Variation of motor flux linkage with position obtained in Ansys CAD

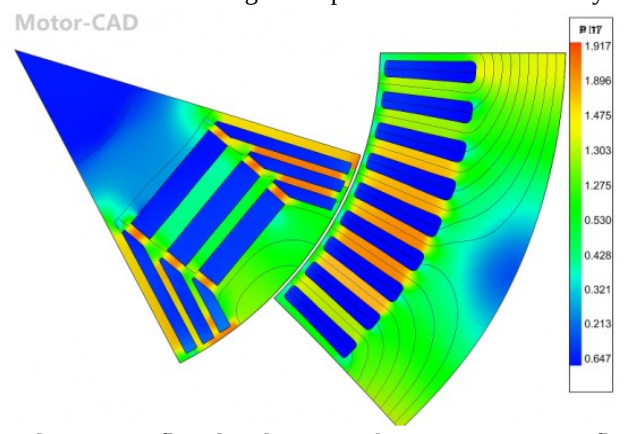


Figure 13: Simulated magnetic flux distribution with varying magnetic flux density obtained from Ansys CAD software

This visual representation shows the magnetic flux density distribution within the rotor geometry. The crucial aspect here is the clear differentiation between areas of zero flux distribution (blue color) in the flux

barriers and maximum distribution (red color) along the barrier gaps. This distinct anisotropic flux path (high permeability along the d-axis and low permeability along the q-axis) is the core principle behind synchronous

reluctance motors, directly facilitating the production of high reluctance torque.

SynRM operating region

Consider Figure 14, the motor shows constant torque operation below rated speed (region 1) and linear increase of power with speed. In region 2 above the base speed, the motor shows exponential decrease of power and torque as speed increases. The operating regions 1 and 2 show a wide speed range of the designed motor.

Based on the operating region, Figure 15 shows the map distribution of electromagnetic torque of the shaft with speed.

This contour map graphically illustrates the electromagnetic torque distribution on the motor's shaft across its operating speed range. It clearly shows a constant torque region (200Nm) from zero speed up to the base speed (8000 rpm), which then begins to decrease beyond this point. Overlaying these torque values are efficiency contours which demonstrate that the motor achieves its highest efficiency when operating at or near its base speed. This map effectively visualizes the motor's operating envelope and its suitability for HEV applications requiring both constant torque and constant power regions, as described in Figure 14.

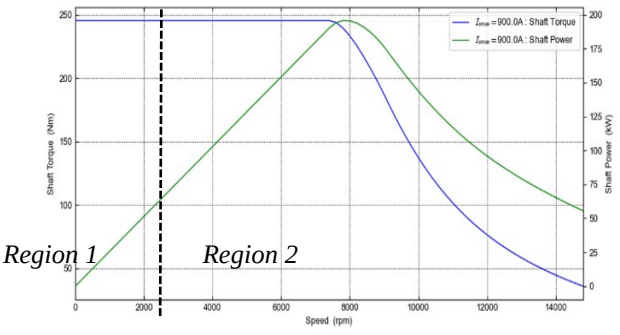


Figure 14: Operating regions of the SynRM

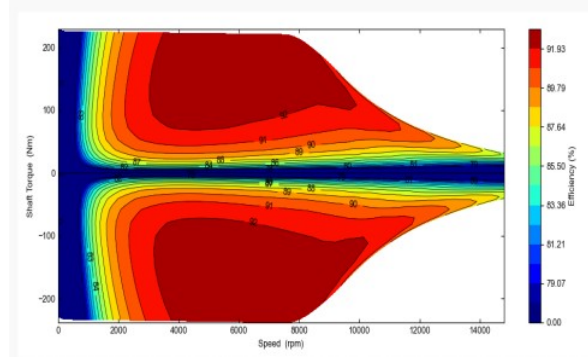


Figure 15: Simulated torque map distribution to show how the different motor speed affect the shaft torque and motor efficiency

Similar to the torque map, Figure 16 displays the mechanical power delivered on the shaft as a function of speed, also with overlaid efficiency contours. It shows a linear increase in mechanical power from 0 rpm up to the base speed. The map also highlights the machine's capability to function effectively as both a motor and a generator with consistent

operating characteristics, and it reiterates that the best operating efficiency is achieved at base speed. This figure complements the torque map by providing a comprehensive view of the motor's power delivery capabilities and efficiency across its operational range.

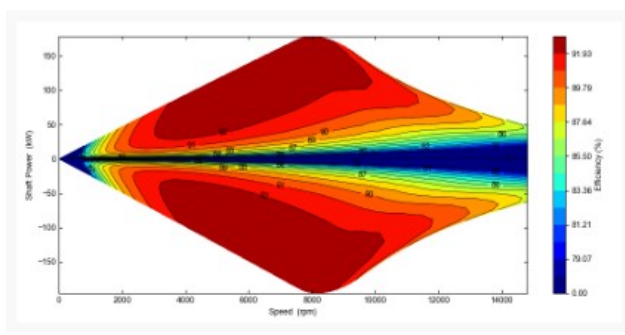


Figure 16: Mechanical power distribution of SynRM in Ansys CAD software with a different speeds

Conclusion

paper successfully This presented a simulation-based design and performance analysis of a high-performance synchronous motor (SvnRM) reluctance specifically tailored for hybrid electric vehicle applications, targeting 75kW nominal and 125kW peak power. Through meticulous rotor and stator geometric optimization, particularly focusing on flux barrier angles and employing comprehensive FEA using Ansys Motor-CAD, the designed motor demonstrated high efficiency, wide operating range, and reduced torque ripple. The absence of rotor winding in the robust rotor design and proper arrangement flux barrier has led to more than 30% reduction in copper losses, improved thermal performance, increased mechanical robustness, and simplified manufacturing processes compared to the induction motor. Moreover, the results indicate that the optimized SvnRM design achieves competitive performance metrics, including a constant torque region up to 8000 rpm and high efficiency at base speed, validating its viability as a robust and rare-earth-free alternative for HEV powertrains. While the comprehensive performance characterization was conducted through advanced simulation, future work will focus on experimental prototyping and validation to corroborate findings and further explore manufacturing feasibility and thermal performance under real-world conditions.

Conflicts of Interest

Authors declare that no conflicts of interest. **Acknowledgements**

The author appreciates the support from the Department of Electrical Engineering, University of Dar es Salaam.

References

Abid S, Shah A, Zanjani SS, Leghari IA and Bhatti JI 2020 The Design and Optimization of Synchronous Reluctance Motor Drive System for Low-Speed Direct-Drive Mining Applications. *Quaid-e-Awam Univ. Res. J. Eng. Sci. Technol.* 18(1): 19–28. Retrieved from http://publications.quest.edu.pk/ojs-3.1.1 4/index.php/qrj/article/view/177

Aghazadeh H, Afjei E and Siadatan A 2019 Comprehensive Design Procedure and Manufacturing of Permanent Magnet Assisted Synchronous Reluctance Motor. *Int. J. Eng. Trans. C: Aspects.*, 32(9): 1299–1305.

https://doi.org/10.5829/ije.2019.32.09c.10 Ayad Alkhafaji, M and Uzun, Y 2018 Design and Analysis of Synchronous Reluctance Motor (SynRM) Using MATLAB/Simulink, 66–79. https://doi.org/10.33422/irset.2018.12.32

Credo A and Pescetto P 2020 Design optimization of a synchronous reluctance motor based on operating cvcle. **Proceedings** 2020 International Conference on Electrical Machines, **ICEM** 2020. 2486–2492. https://doi.org/10.1109/ICEM49940.2020. 9271012

Duc HB, Chi DD, Do P-C and Quoc VD 2023 Modeling of Synchronous Reluctance Motors by Analytical and Finite Element Approaches for Electric Vehicle Applications. *J. Sci. Technol.*

- Issue Inform. Commun. Technol. 21(6): 39–44. https://doi.org/10.31130/ud-jst.2023.085ict
- Dursun DC, Yildiz A and Polat M 2023 International Conference on Advances and Innovations in Recycling Engineering , AIR 2021 Lecture Notes in Civil Engineering, 301 LNCE(October).
- Hu Y, Chen B, Xiao Y, Shi J and Li L 2020 Study on the Influence of Design and Optimization of Rotor Bars on Parameters of a Line-Start Synchronous Reluctance Motor. *IEEE Trans. Ind. Appl.*, 56(2), 1368–1376. https://doi.org/10.1109/TIA.2019.296243
- Hu Y, Chen B, Xiao Y, Shi J, Li X and Li L 2021 Rotor Design and Optimization of a Three-Phase Line-Start Synchronous Reluctance Motor. *IEEE Trans. Ind. Appl.*, 57(2): 1365–1374. https://doi.org/10.1109/TIA.2020.304322
- Hua Y, Zhu H, Gao M and Ji Z 2021 Design and analysis of two permanent-magnet-assisted bearingless synchronous reluctance motors with different rotor structure. *Energies*, 14(4). https://doi.org/10.3390/en14040879
- Jung JW, Dang DQ, Thi-Thuy Vu, N, Justo JJ, Duc Do T, Choi HH, and Kim TH 2015 A nonlinear sliding mode controller for IPMSM drives with an adaptive gain tuning rule. *J Power Electron.*, 15(3): 753–762.
- https://doi.org/10.6113/JPE.2015.15.3.753
 Kim Y, Koo B and Nam K 2019 Induction
 Motor Design Strategy for Wide Constant
 Power Speed Range. *IEEE Trans. Ind. Electron.*, 66(11): 8372–8381.
 https://doi.org/10.1109/TIE.2018.2885691
- Kocan S, Rafajdus P, Bastovansky R, Lenhard R and Stano M (2021). Design and optimization of a high-speed switched reluctance motor. *Energies*, 14(20).

https://doi.org/10.3390/en14206733

J. K. Kostko, "Polyphase reaction synchronous motors," in Journal of the American Institute of Electrical Engineers, vol. 42, no. 11, pp. 1162-1168, Nov. 1923, doi:

- 10.1109/JoAIEE.1923.6591529.
- Kuci E, Henrotte F, Geuzaine C, Dehez B, Greef C, De Versele C and Friebel C 2020 Design optimization of synchronous reluctance machines for railway traction application including assembly process constraints. *Proceedings 2020 International Conference on Electrical Machines, ICEM 2020,* 117–123. https://doi.org/10.1109/ICEM49940.2020. 9270859
- Liu CT, Shih PC, Cai ZH, Yang K, Yen SC, Lin HN, Lin SY 2019 Designs of a four-in-one laminated electrical steel rotor structure for application-oriented synchronous reluctance motors. *IEEE Trans. Ind. Appl.*, 55(4): 4389–4397.

https://doi.org/10.1109/ TIA.2019.2911569

Liu Z, Hu Y, Wu J, Zhang B and Feng G 2021 A Novel Modular Permanent Magnet-Assisted Synchronous Reluctance Motor. *IEEE Access*, 9: 19947–19959.

https://doi.org/10.1109/

ACCESS.2021.3054766

- Myint ZH 2018 Design Consideration of Permanent Magnet Synchronous Reluctance Motor by Finite Element Method. *Int. J. Sci. Eng. Appl.* 7(8): 181–186.
- https://doi.org/10.7753/ijsea0708.1011 R. -R. Moghaddam, F. Magnussen and C. Sadarangani. "Novel rotor optimization of Synchronous Reluctance Machine for low torque ripple," 2012 XXth International Conference Electrical Machines, Marseille, France, 2012, pp. 720-724, doi: 10.1109/ICElMach.2012.6349952.
- Tursini M, Villani M, Fabri G, Credo A, Parasiliti F and Abdelli A Synchronous Reluctance Motor: Design, Optimization and Validation. SPEEDAM **International** 2018 **Proceedings:** Power **Symposium** on Electronics. Electrical Automation Drives, and Motion. (June), 1297-1302. https://doi.org/10.1109/SPEEDAM.2018. 8445304

Wang Y, Bacco G and Bianchi N 2017)

Geometry Analysis and Optimization of PM-Assisted Reluctance Motors. *IEEE Trans. .Ind. Appl.*, 53(5): 4338–4347. https://doi.org/10.1109/TIA.2017.2702111

Yamazaki K, Kato Y, Ikemi T and Ohki S 2014 Reduction of rotor losses in multilayer interior permanent-magnet synchronous motors by introducing novel topology of rotor flux barriers. *IEEE Trans. Ind. Appl.*, 50(5): 3185–3193. https://doi.org/10.1109/TIA.2014.230342

Zhu X, Wu W, Yang S, Xiang Z and Quan L 2018 Comparative design and analysis of new type of flux-intensifying interior permanent magnet motors with different Q-axis rotor flux barriers. *IEEE Trans. Energ. Convers.*, 33(4): 2260–2269. https://doi.org/10.1109/TEC.2018.2837119